Representation Learning for Clustering via Building Consensus

Aniket Anand Deshmukh, Jayanth Reddy Regatti, Eren Manavoglu, and Urun Dogan

Abstract—In this paper, we focus on deep clustering and unsupervised representation learning for images. Recent advances in deep clustering and unsupervised representation learning are based on the idea that different views of an input image (generated through data augmentation techniques) must be closer in the representation space (exemplar consistency), and/or similar images have a similar cluster assignment (population consistency). We define an additional notion of consistency, consensus consistency, which ensures that representations are learnt to induce similar partitions for variations in the representation space, different clustering algorithms or different initializations of a clustering algorithm. We define a clustering loss by performing variations in the representation space and seamlessly integrate all three consistencies (consensus, exemplar and population) into an end-to-end learning framework. The proposed algorithm, Consensus Clustering using Unsupervised Representation Learning (ConCURL) improves the clustering performance over state-of-the art methods on four out of five image datasets. Further, we extend the evaluation procedure for clustering to reflect the challenges in real world clustering tasks, such as clustering performance in the case of distribution shift. We also perform a detailed ablation study for a deeper understanding of the algorithm.

1 Introduction

The field of artificial intelligence (AI) advanced significantly in the previous decade due to developments in deep learning [1]. In the early years, deep learning methods showed stellar performance for supervised learning where each data sample is coupled with ground truth (labelled data) e.g., each image is associated with a category. Unfortunately generating labelled data sets is time consuming, expensive and there may not exist enough experts for labelling the data at hand (e.g. medical images). The straightforward solution is to use clustering for large-scale problems.

In this work, we focus on representation learning for the unsupervised learning task of clustering images. Clustering is an ubiquitous task and it has been actively used in many different scientific and practical pursuits [2], [3], [4], [5]. These clustering algorithms do not learn the representations and are hence limited to data for which we have a good representation available.

Advancements in deep learning techniques have enabled end-to-end learning of rich representations of images for supervised learning. For the purposes of clustering, however, such features learned via supervised learning can not be obtained due to lack of availability of labels. Therefore, supervised learning approaches fall short of providing a solution. Self-supervised learning addresses the issue of learning representations without labeled data. Self-supervised learning is a sub-field of unsupervised learning in which the main goal is to learn general purpose representations by exploiting user-defined tasks (pretext tasks) [6], [7], [7], [8], [9], [10], [11]. These representation learning algorithms were shown to achieve good results when evaluated using linear evaluation protocol, semi-supervised training on ImageNet, or transfer to

- Jayanth Reddy Regatti is with Ohio State University.
- Aniket Anand Deshmukh, Eren Manavoglu, and Urun Dogan are with Microsoft.

Manuscript received April 30, 2021.

downstream tasks. A straight forward solution to the clustering problem is to use the features learned using self-supervised learning, and apply an out-of-the-box clustering algorithm (such as k-means) to compute clusterings of the data. However, the performance of these features for clustering (using an out-of-the-box clustering algorithm) is not known, and as seen in our results these features may be improved for clustering.

On the other hand, deep clustering involves simultaneously learning cluster assignments and features using deep neural networks. Simultaneously learning the feature spaces with a clustering objective in deep clustering may lead to degenerate solutions, which until recently limited end-to-end implementations of clustering with representation learning approaches [12]. Subsequently, there have been several works [12], [13], [14], [15], [16], [17], [18], [19]. We give details of some of these works in the Section 1.1. We categorize current clustering and representation learning works based on consistency constraints that are used to define the objective function of these works. We define an additional notion of consistency, consensus consistency, which ensures that representations are learnt to induce similar partitions for variations in the representation space, different clustering algorithms or different initializations of a clustering algorithm. We use consensus consistency and propose an end-to-end learning approach which outperforms other end-to-end learning methods for image clustering. We summarize our contributions as follows:

- We introduce the different notions of consistency (exemplar, population and consensus) used in unsupervised representation learning.
- We propose a novel clustering algorithm that incorporates the three consistency constraints and can be trained in an end-to-end way. The ensemble in the consensus clustering objective is generated by performing random transformations on the embeddings.
-) We show that the proposed algorithm ConCURL (Con-

- sensus Clustering with Unsupervised Representation Learning) outperforms baselines on popularly used computer vision datasets evaluated for clustering metrics.
- 4) We show clustering ability of trained models under data shift and argue the need of different evaluation metrics for deep clustering algorithms.
- 5) We study the impact of hyper-parameters, data augmentations, resolution of images on the clustering ability of the proposed algorithm.

1.1 Related Work

Self-supervised Learning: Self-supervised learning is used to learn representations in an unsupervised way by defining some pretext tasks. There are many different flavors of self-supervised learning such as instance discrimination tasks [6], [7] and contrastive techniques [8], [9]. In instance discrimination tasks, each image is considered as its own category so that the learned embeddings are well separated [6]. Building on the Instance Discrimination (ID) task, Zhuang et al., [7] propose a Local Aggregation (LA) method based on a robust clustering objective (using multiple runs of k-means) to move statistically similar data points closer in the representation space and dissimilar data points further away. In contrastive techniques such as SimCLR [9], MoCo [20], representations are learned by maximizing agreement between different augmented views of the same data example (known as positive pairs) and minimizing agreement between augmented views of different examples (known as negative pairs). Recent works BYOL [10], SwAV [11] achieve state-of-the-art results without requiring negative pairs. Although self-supervised learning methods show impressive performance on a variety of problems, it is not clear whether learned representations are good for clustering.

Clustering with Representation Learning: DEC [13] is one of the first algorithms to show deep learning can be used effectively to cluster images in an unsupervised way, where they use features learned from an autoencoder to finetune the cluster assignments. DeepCluster [12] shows that it is possible to train deep convolutional neural networks end-to-end with pseudo labels that are generated by a clustering algorithm. Subsequently, there have been several works [14], [15], [16], [17], [18] that introduce end-to-end clustering based objectives and achieve state-of-the-art clustering results. For example, in Gaussian ATtention network for image clustering (GATCluster) [16], training is performed in two distinct steps, similar to [12] where the first step is to compute pseudo targets for a large batch of data and the second step is to train the model in a supervised way using the pseudo targets. Both DeepCluster and GATCluster use k-means to generate pseudo labels which may not scale well. [17] propose Deep Comprehensive Correlation Mining (DCCM), where discriminative features are learned by taking advantage of the correlations of the data using pseudo-label supervision and triplet mutual information among features. However, DCCM may be susceptible to trivial solutions [16]. Invariant Information Clustering (IIC) [15] maximizes mutual information between the class assignments of two different views of the same image (paired samples) in order to learn representations that preserve what is common between the views while discarding instance specific details. It is argued that the presence of an entropy term in mutual information plays an important role in avoiding the degenerate solutions. However a large batch size is needed for the computation of mutual information in IIC, which may not be scalable for larger image sizes which are common in popular datasets [15], [16]. [18] extend the celebrated maximal margin clustering idea to the deep learning paradigm, by learning the most semantically plausible clustering through minimizing a proposed partition uncertainty index. Their algorithm PICA uses a stochastic version of the index, thereby facilitating mini-batch training. PICA fails to assign a sample-correct cluster when that sample either has high foreground or background similarity to samples in other clusters. In a more recent approach contrastive clustering [21], contrastive learning loss like in SimCLR [9] was adopted along with entropy term to avoid the degenerate solution. Similarly, [19] combines instance discrimination [6] with a novel softmax-formulated decorrelation constraints for representation learning and clustering. Their approach outperforms state of the art methods and improves on instance discrimination method. Our method also improves on instance discrimination and outperforms [19] on all datasets considered. There are other non end-to-end approaches such as SCAN [22] which use the learned representations from a pretext task to find semantically closest images to the given image using nearest neighbors.

2 Consensus Clustering

One of the distinguishing factors between supervised learning and unsupervised learning is the existence of ground-truth labels which construct a global constraint over examples. In most of the self-supervised learning methods, ground-truth is replaced with some consistency constraint [9]. Without a doubt, the performance of any self-supervised method is a function of the power of the used consistency constraint. We define two types of consistency constraints - exemplar consistency and population consistency.

Definition 1. Exemplar consistency: Representation learning algorithms that learn closer representation (in some distance metric) for different augmentations of the same data point are said to follow exemplar consistency.

Examples of usage of exemplar consistency include contrastive learning methods like MoCo [20], SimCLR [9], etc. In these methods, positive pairs of images are defined as any two image augmentations of the same image and negative pairs are any two different images.

Definition 2. *Population consistency:* Representation learning algorithms which ensure learned representations satisfy the consistency constraint that two similar data points or any augmentation of the same data points should belong to the same cluster (or population) are said to follow population consistency.

Deep Cluster [12] is a prominent self-supervised method which utilizes a population consistency, i.e. Definition 2, by enforcing a clustering on the data set. Please note that each cluster assignments contain data points that are similar to each other. Similarly, SwAV [11] is an example of population consistency method.

Definition 3. Consensus consistency: Representation learning algorithms which are able to learn representations that induce similar partitions for variations in the representation space (subsets of features, random projection, etc.), different clustering algorithms (k-means, GMM, etc.) or different initialization of clustering algorithms are said to follow consensus consistency.

Earlier works on *consensus consistency* do not consider representation learning and use the knowledge reuse framework (see

[23], [24]) where the cluster partitions are available (features are irrelevant) or the features of the data are fixed. For example, Fern and Brodley [25], successfully applied Random Projections to Consensus Clustering, by performing k-means clustering on multiple random projections of the fixed features of input data. In contrast, the notion of consensus consistency here deals with learning representations that achieve a consensus on the cluster assignments of multiple clustering algorithms. One example of methods that enforce consensus consistency is Local Aggregation (LA) [7]. LA builds on ID task [6] and proposes a method based on a robust clustering objective (using multiple runs of k-means) to move statistically similar data points closer in the representation space and dissimilar data points further away. However, Zhuang et al. [7] does not evaluate for clustering metrics and only focuses on linear evaluation using the learned features. Subsequently, we conducted a study to evaluate the clustering performance of these features (see Appendix) and observe that LA performs poorly when evaluated for clustering accuracy. In Definition 3, we inherently assume that the clustering algorithms under considerations have been tuned properly. Unfortunately, the definition of consensus consistency is ill-posed, there can be arbitrarily many different partitions which can satisfy the given condition¹. We show that when exemplar consistency used as an inductive bias the resulting objective function shows impressive performance on challenging data sets. Combining exemplar and population constraints with consensus consistency seamlessly and effectively for clustering is the basis of our proposed method.

2.1 Loss for Consensus and Population Consistency

We are focused on learning generic representations that satisfy Definition 3 for clustering. By using different clustering algorithms or different variations in representation (such as projections), one can easily generate multiple different partitions of the same data. In unsupervised learning, it is not known which partitioning is correct. To tackle this problem some additional assumptions are needed.

We assume that there is an underlying latent space \mathcal{Z}^* (possibly not unique) such that all clusterings (based on variation of latent space, algorithm or initialization) that take input data from this latent space produce similar partitions of the data. Furthermore, every clustering algorithm that also takes the true number of clusters as input, produces the partition that is closest to the hypothetical ground truth. Moreover, we are assuming that there exists a function $h: X \to \mathcal{Z}^*$, where X represents the input space and \mathcal{Z}^* represents the underlying latent space. We call this assumption the **principle of consensus**. The open question is how one constructs an efficient loss which reflects the **principle of consensus**. We define one such way below.

Given an input batch of images $\mathcal{X}_b \subset \mathcal{X}$, the goal is to partition these images into K clusters. We get p views (by different image augmentations) of these images and define a loss such that cluster assignment of any of the p views match the targets estimated from any other view. Without loss of generality we define a loss for p=2 views. The two views $\mathcal{X}_b^1, \mathcal{X}_b^2$ are generated using two randomly chosen image augmentations. We learn a representation space \mathcal{Z}_0 at the end of every training iteration and get M variations of \mathcal{Z}_0 as $\{\mathcal{Z}_1, \mathcal{Z}_2, ..., \mathcal{Z}_M\}$ (e.g.

random projections, etc). The goal is to build an efficient loss by the **principle of consensus** among \mathcal{Z}_0 and it's M variations $\{\mathcal{Z}_1,\mathcal{Z}_2,...,\mathcal{Z}_M\}$ such that we learn the latent space \mathcal{Z}^* at the end of training (i.e. the learned features lie in the latent space described above). For a given batch of images \mathcal{X}_b and representation space $\mathcal{Z}_m, \forall m \in [0,1,...,M]$, we denote the cluster assignment probability for image i and cluster j for view 1 as $\mathbf{p}^1_{i,j}(\mathcal{Z}_m)$ and for view 2 as $\mathbf{p}^2_{i,j}(\mathcal{Z}_m)$. Here we define the loss that incorporates "population consistency" and "consensus consistency". We assume that oracle has given us target cluster assignment probabilities for the representation \mathcal{Z}_0 (like in Deep-Cluster [12]) and denote it as $\mathbf{q}^1_{i,j}$ for view 1 and $\mathbf{q}^2_{i,j}$ for view 2.

We define loss for any representation space \mathcal{Z} and batch of images \mathcal{X}_b as

$$L_{\mathcal{Z}}^{1} = -\frac{1}{2B} \sum_{i=1}^{B} \sum_{j=1}^{K} \mathbf{q}_{ij}^{2} \log \mathbf{p}_{ij}^{1}(\mathcal{Z})$$

$$L_{\mathcal{Z}}^{2} = -\frac{1}{2B} \sum_{i=1}^{B} \sum_{j=1}^{K} \mathbf{q}_{ij}^{1} \log \mathbf{p}_{ij}^{2}(\mathcal{Z}), \qquad (1)$$

$$L_{\mathcal{Z}} = \sum_{i=0}^{M} \left(L_{\mathcal{Z}_{i}}^{1} + L_{\mathcal{Z}_{i}}^{2} \right).$$

Note that, here consensus over the clusterings is defined via common targets \mathbf{q} . The exact details of how to get variations of \mathcal{Z}_0 , calculate cluster assignment probabilities \mathbf{p} and targets \mathbf{q} are described in the next section.

2.2 End-to-End SGD Trainable Consensus Loss

In this section we propose an end-to-end trainable algorithm and define a way to compute \mathbf{p} and \mathbf{q} . When cluster assignment probabilities \mathbf{p} can take any value in the set [0,1] then we refer to it as soft clustering and when \mathbf{p} is restricted to the set $\{0,1\}$ then we refer to it as hard clustering. The proposed method can be used with hard clustering and soft clustering.

Without loss of generality, in this paper, we focus on soft clustering which makes it easier to define a loss using the probabilities and update the parameters using the gradients to enable end-to-end learning. We follow the soft clustering framework presented in SwAV [11], which is a centroid based technique and aims to maintain consistency between the clusterings of the augmented views \mathcal{X}_b^1 and \mathcal{X}_b^2 . We store a set of randomly initialized prototypes $C_0 = \{\mathbf{c}_0^1, \cdots, \mathbf{c}_0^K\} \in \mathbb{R}^{d \times K}$, where K is the number of clusters, and d is the dimension of the prototypes. These prototypes are used to represent clusters and define a "consensus consistency" loss. We compute M variations of C_0 as $C_1, ..., C_M$ exactly like we compute M variation of \mathcal{Z}_0 .

2.2.1 Cluster assignment probability p

We use a two layer MLP g to project the features $\mathbf{f}^1 = f_{\theta}(\mathcal{X}_b^1)$ and $\mathbf{f}^2 = f_{\theta}(\mathcal{X}_b^2)$ to a lower dimensional space \mathcal{Z}_0 (of size d). The output of this MLP (referred to as cluster embeddings) is denoted using $Z_0^1 = \{\mathbf{z}_0^{1,1},\ldots,\mathbf{z}_0^{1,B}\}$ and $Z_0^2 = \{\mathbf{z}_0^{2,1},\ldots,\mathbf{z}_0^{2,B}\}$ for view 1 and view 2 respectively. Note that $h: \mathcal{X} \to \mathcal{Z}$ defined in 2.1 is equivalent to composite function of $f: \mathcal{X} \to \Phi$ and $g: \Phi \to \mathcal{Z}$. For a latent space \mathcal{Z} , we compute the probability of assigning a cluster j to image i using the normalized vectors $\bar{\mathbf{z}}^{1,i} = \frac{\mathbf{z}^{1,i}}{||\bar{\mathbf{z}}^{1,i}||}, \bar{\mathbf{z}}^{2,i} = \frac{\mathbf{z}^{2,i}}{||\mathbf{z}^{2,i}||}$ and $\bar{\mathbf{c}}_j = \frac{\mathbf{c}^j}{||\mathbf{c}^j||}$ as

^{1.} a) Degenerate solution where all clusters assignments are the same, b) Random assignment can satisfy this condition given that all clustering are producing the same but random assignments

$$\mathbf{p}_{i,j}^{1}(\mathcal{Z},C) = \frac{\exp(\frac{1}{\tau}\langle \mathbf{\bar{z}}_{i}^{1}, \mathbf{\bar{c}}_{j}\rangle)}{\sum_{j'} \exp(\frac{1}{\tau}\langle \mathbf{\bar{z}}_{i}^{1}, \mathbf{\bar{c}}_{j'}\rangle)},$$

$$\mathbf{p}_{i,j}^{2}(\mathcal{Z},C) = \frac{\exp(\frac{1}{\tau}\langle \mathbf{\bar{z}}_{i}^{2}, \mathbf{\bar{c}}_{j}\rangle)}{\sum_{i'} \exp(\frac{1}{\tau}\langle \mathbf{\bar{z}}_{i}^{2}, \mathbf{\bar{c}}_{i'}\rangle)}.$$
(2)

We concisely write $\mathbf{p}_i^1(\mathcal{Z}) = \{\mathbf{p}_{i,j}^1(\mathcal{Z},C)\}_{j=1}^K$ and $\mathbf{p}_i^2 = \{\mathbf{p}_{i,j}^2(\mathcal{Z},C)\}_{j=1}^K$. Here, τ is a temperature parameter and we set the value to 0.1 similar to Caron *et al.*, [11]. Note that, we use \mathbf{p}_i to denote the predicted cluster assignment probabilities for image i (when not referring to a particular view), and a shorthand \mathbf{p} is used when i is clear from context.

2.2.2 Targets q

The idea of predicting assignments **p**, and then comparing them with high-confidence estimates **q** (referred to as codes henceforth) of the predictions was proposed in Xie *et al.*, [13]. While Xie *et al.*, [13] uses pretrained features (from autoencoder) to compute the predicted assignments and the codes, using their approach in an end-to-end unsupervised manner might lead to degenerate solutions. Asano *et al.*, [26] avoid such degenerate solutions by enforcing an equi-partition constraint (the prototypes equally partition the data) during code computation using the Sinkhorn-Knopp algorithm [27]. Caron *et al.*, [11] follow a similar formulation but compute the codes for the two views separately in an online manner for each mini-batch. The assignment codes are computed by solving the following optimization problem

$$\begin{split} Q^1 &= \mathop{\arg\max}_{Q \in \mathcal{Q}} \mathrm{Tr}(Q^T C_0^T Z_0^1) + \epsilon H(Q) \\ Q^2 &= \mathop{\arg\max}_{Q \in \mathcal{Q}} \mathrm{Tr}(Q^T C_0^T Z_0^2) + \epsilon H(Q), \end{split} \tag{3} \end{split}$$

where $Q = \{\mathbf{q}_1, \dots, \mathbf{q}_B\} \in \mathbb{R}_+^{K \times B}$, Q is the transportation polytope defined by

$$\mathcal{Q} = \{\mathbf{Q} \in \mathbb{R}_+^{K \times B} | \mathbf{Q} \mathbf{1}_B = \frac{1}{K} \mathbf{1}_K, \mathbf{Q}^T \mathbf{1}_K = \frac{1}{B} \mathbf{1}_B \}$$

 $\mathbf{1}_K$ is a vector of ones of dimension K and $H(Q) = -\sum_{i,j} Q_{i,j} \log Q_{i,j}$. The above optimization is computed using a fast version of the Sinkhorn-Knopp algorithm [27] as described in Caron *et al.*, [11].

After computing the codes Q^1 and Q^2 , in order to maintain consistency between the clusterings of the augmented views, the loss is computed using the probabilities \mathbf{p}_{ij} and the assigned codes \mathbf{q}_{ij} by comparing the probabilities of view 1 with the assigned codes of view 2 and vice versa like in equation 1.

2.2.3 Defining variations of Z_0 and C_0

To compute $\{Z_1,...,Z_M\}$, we project d dimensional space Z_0 to a D dimension space using random projection matrix. We follow the same procedure to compute $\{C_1,...,C_M\}$ from C_0 . At the beginning of the algorithm, we randomly initialize M such transformations and fix them throughout training. Suppose using a particular random transformation (a randomly generated matrix A), we get $\tilde{\mathbf{z}} = A\mathbf{z}$, $\tilde{\mathbf{c}} = A\mathbf{c}$. We then compute the softmax probabilities using the normalized vectors $\tilde{\mathbf{z}}/||\tilde{\mathbf{z}}||$ and $\tilde{\mathbf{c}}/||\tilde{\mathbf{c}}||$. Repeating this with the M transformations results in M predicted cluster assignment probabilities for each view. When the network is untrained, the embeddings \mathbf{z} are random

and applying the random transformations followed by computing the predicted cluster assignments leads to a diverse set of soft cluster assignments. The parameter weights are trained by using the stochastic gradients of the loss for updates.

2.2.4 Backbone Loss

To capture exemplar consistency better and based on previous evidence of successful clustering with Instance Discrimination (ID) approach [19], we use Instance Discrimination (ID) [6] as one of the losses like in [19]. The exemplar objective of ID is to classify each image as it's own class.

Given n images and neural network f_{θ} to calculate features, we first normalize features $\bar{f}_{\theta}(x) = \frac{f_{\theta}(x)}{\|f_{\theta}(x)\|}$. Then ID defines the probability of an example x being recognized as i-th example is

$$P(i|f_{\theta}(x)) = \frac{\exp\left(\langle \bar{f}_{\theta}(x_i), \bar{f}_{\theta}(x)\rangle/\tau\right)}{\sum_{j=1}^{n} \exp\left(\langle \bar{f}_{\theta}(x_j), \bar{f}_{\theta}(x)\rangle/\tau\right)}.$$
 (4)

ID then uses uniform distribution as a noise distribution $P_n = \frac{1}{n}$ to compute a probability of data example x coming from a data distribution P_d as opposed to noise distribution P_n as $h(i,f_{\theta}(x)) := \frac{P(i|f_{\theta}(x))}{P(i|f_{\theta}(x))+mP_n(i)}$. Assuming that noise samples are m times more frequent than actual data samples, ID loss is defined as

$$L_b = -E_{P_d} \left[\log h(i, x) \right] - m E_{P_n} \left[\log (1 - h(i, x')) \right], \quad (5)$$

where x' is the feature from randomly drawn image from a given dataset other than image x. We exactly follow a framework from [6] to implement the ID loss.

The final loss that we sought to minimize is the combination of the losses L_Z (equation 1) and L_b (equation 5),

$$L_{\text{total}} = \alpha L_{\mathcal{Z}} + \beta L_b. \tag{6}$$

where α, β are non-negative constants.

2.2.5 Computing the cluster metrics

In this section, we describe the approach to compute the cluster assignments and the metrics evaluate their quality. Note that we assume the number of true clusters (K) in the data is known.

There are two ways to compute the cluster assignments. The first way is to use the embeddings generated by the backbone, here it is the output of the ID block $f_{\theta}(x)$. The embeddings of all the images are computed and then we perform K-means clustering.

The second way is to use the soft clustering block to compute the cluster assignments. It is sufficient to use the computed probability assignments $\{\mathbf{p}_i\}_{i=1}^N$ or the computed codes $\{\mathbf{q}_i\}_{i=1}^N$ and assign the cluster index as $c_i = \arg\max_k \mathbf{q}_{ik}$ for the i^{th} data point. Once the model is trained, in this second approach, the cluster assignment can be performed online without requiring to compute the embeddings of all the input data.

We evaluate the quality of the clusterings using metrics such as cluster accuracy, NMI, ARI. To compute clustering accuracy, we are required to solve an assignment problem (computed using a Hungarian match [28], [29]) between the true class labels and the cluster assignment. In our analysis, we observe that using K-means with the embeddings of ID block achieved better clustering accuracy and we use this method throughout the paper while evaluating our proposed algorithm.

TABLE 1: Different ways to generate ensembles

Data Representation	Clustering algorithms
Different data preprocessing techniques	Multiple clustering algorithms (k-means, GMM, etc)
Subsets of features	Same algorithm with different parameters or initializations
Different transformations of the features	Combination of multiple clustering and different parameters or initializations

2.3 Generating Multiple Clusterings

Fred and Jain, [30] discuss different ways to generate an ensemble of clusterings which are tabulated in Table 1. In our proposed algorithm, we focus on choosing of data representation to generate cluster ensembles.

By fixing a stable clustering algorithm, we can generate arbitrarily large ensembles by applying different transformations on the embeddings. Random projections were successfully used in Consensus Clustering previously [25]. By generating ensembles using random projections, we have control over the amount of diversity we can induce into the framework, by varying the dimension of the random projection. In addition to Random Projections, we also used diagonal transformations [31] where different components of the representation vector are scaled differently. Hsu *et al.*, [31] illustrate that such scaling enables a diverse set of clusterings which is helpful for their meta learning task. We study the ablations over number of transformations needed and dimension of these transformations in the section 5.

3 Understanding the Consensus Objective

We investigate a potential hypothesis of "training driven by noisy cluster assignments" that can shed light on the success of Con-CURL ². The hypothesis stems from the following intuition: *Using different clustering algorithms, the generated cluster assignments are noisy versions of the hypothetical ground truth; as training progresses, the noise in the cluster assignments reduces and eventually all different clustering algorithms considered generate similar cluster assignments*.

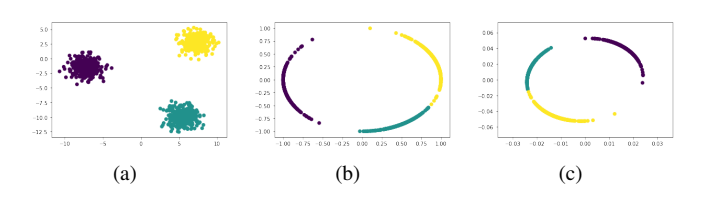


Fig. 1: a: Three cluster dataset = z, b: Normalized data, c: Transformed and then Normalized Data

We verify this hypothesis empirically with the help of the following experiments on STL-10 dataset: (i) observe noisy clusterings generated by using Random Projections and (ii) verify that the noise in the cluster assignments reduces as training progresses.

For the purpose of demonstrating noisy cluster assignments, we use synthetic data as follows. We generate three clusters in

2. A theoretically grounded explanation of ConCURL is considered as a future work due to the non-convexity of deep learning methods and non-convexity of proposed loss.

 \mathbb{R}^2 as shown in Fig 1(a) and compute the centroids of each cluster. Here, the centroids act as the prototypes. We then generate a Gaussian Random Projection matrix A of dimension $\mathbb{R}^{2\times 2}$. We first normalize the embeddings (2 dim features) and the centroids (see Fig 1(b)). Using the matrix A, we transform both the embeddings and prototypes to the new space and normalize the resultant vectors (see Fig 1(c)).

We follow the soft clustering framework discussed earlier and compute the soft cluster assignments for the original and the transformed data. We observe that, these probability of cluster assignments in the new space are a noisy version of probability of cluster assignments in the original space (see Table 2).

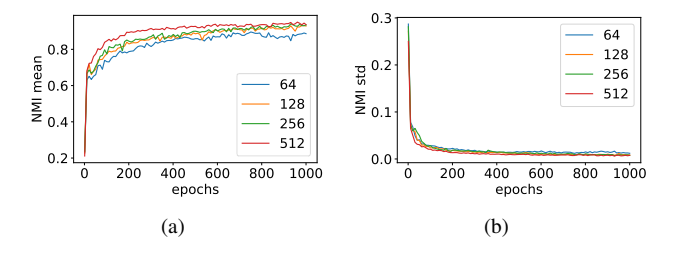


Fig. 2: Pairwise NMI as a way to measure the diversity in the ensemble. The results are for STL-10 dataset, and shows pairwise NMI for different random projection dimensions (the original dimension of **z** is 256).

To verify that the noise in the cluster assignment probabilities reduces as training progresses, we perform the following experiment. We measure the similarity in cluster assignments at every epoch to observe the effect of consensus as training progresses. For each random projection used, we use cluster assignment probabilities $\tilde{\mathbf{p}}$ and compute cluster assignments by taking an $\arg\max$ on $\tilde{\mathbf{p}}$ of each image. We get M such cluster assignments due to the M random projections. We then compute a pairwise NMI (Normalized Mutual Information) (similar analysis to Fern and Brodley, [25]) between every two cluster assignments, and compute the average and standard deviation of the pairwise NMI across the $\frac{M(M-1)}{2}$ pairs. An NMI score of 1.0 signifies that the two clusterings perfectly correlate with each other, and a score of 0.0 implies that the two clusterings are uncorrelated. We observe from Figure 2 that the pairwise NMI increases as training progresses and becomes closer to 1. At the beginning of training, the cluster assignments are very diverse (small NMI score with a larger standard deviation); and as training progresses, the diversity is reduced (large NMI score with a smaller standard deviation). This observation leads us to conclude that for the clustering algorithms (defined using different random projections) we have learned an embedding space where the different cluster assignments concur. In other words, "consensus consistency" is achieved. Also, it is evident from our empirical results in Section 4 that we achieve better clustering accuracy overall.

If noisy cluster assignments are to be the reason behind the improved performance, one might wonder if it is sufficient to simply add noise to the original cluster assignments rather than computing multiple cluster assignments. However this may not be fruitful because if noise is added externally, one will have to define a scheduler to reduce the noise as training progresses. But in the case of ConCURL, end-to-end learning algorithm figures out the rate of consensus or agreement between ${\bf p}$ and $\tilde{{\bf p}}$ itself. In the next section we give empirical evidence of the effectiveness of

TABLE 2: Predicted cluster assignment probability and target probability from Sinkhorn algorithm for four data points

Cluster assignment probability p

	Craster assig	,proou	erney p
	Cluster 1	Cluster 2	Cluster 3
1	0.6473	0.2587	0.0940
2	0.7180	0.1812	0.1008
3	0.0832	0.3160	0.6008
4	0.1543	0.5917	0.2541

Cluster assignment probability $\tilde{\mathbf{p}}$

	Cluster 1	Cluster 2	Cluster 3
1	0.6764	0.2271	0.0965
2	0.7305	0.1680	0.1015
3	0.0802	0.3371	0.5827
4	0.1357	0.5784	0.2860

targets q from sinkhorn

	cluster 1	cluster 2	cluster 3
1	1.0	8.9e-09	1.7e-17
2	1.0	9.1e-13	8.7e-18
3	6.8e-18	2.2e-6	1.0
4	2.5 e-12	1.0	5.4e-8

our method.

4 EMPIRICAL EVALUATION

Evaluating clustering algorithms is a notoriously hard. As the reference text [32] puts it: The validation of clustering structures is the most difficult and frustrating part of cluster analysis. Without a strong effort in this direction, cluster analysis will remain a black art accessible only to those true believers who have experience and great courage.

In the representation learning for clustering literature, e.g. [19], [21], [33], for evaluating performance of different algorithms the following methodology has been used: as set of models with some hyper-parameters are trained and these models are sorted by the observed clustering performance. Finally the best model's results are reported. This methodology will be named as max-performance in the remaining of the paper. We assess the quality of learned embeddings by using five challenging image data sets for clustering and report their performance with maxperformance strategy. Although max-performance procedure gives some insights about the performance of the method under consideration, we give additional insights by significantly extending the evaluations. In practice, it is desirable that learned models can be utilized for different dataset other than the training dataset. To assess the performance of ConCURL, we have designed two additional experiments that focuses on performance of cross-model features and performance of ConCURL under distribution shift. Furthermore, we also assess the quality of the learned embeddings in image retrieval tasks. Finally, we present detailed ablation study to assess the impact of data augmentations, hyper-parameters and architecture choice in order to have a more complete picture.

4.1 Image Clustering max-performance

We evaluated our algorithm and compared against existing work on some popular image data sets namely ImageNet-10, ImageNet-Dogs, STL-10, CIFAR-10, CIFAR100-20. For CIFAR100-20, we used the 20 meta classes as the class labels while evaluating clustering. For STL-10 similar to earlier approaches PICA [18] and GATCluster [16], we used both train and test splits for training and evaluation. Note that PICA also uses unlabelled data split of 100k points in STL-10 which we don't use. ImageNet-10 and ImageNet-Dogs are subsets of ImageNet and we only used train split for these two datasets [34]. We used the same classes as [35] for evaluating on ImageNet-10 and ImageNet-Dogs datasets. The dataset summary is given in Table 3. We evaluate for the cluster accuracy, NMI, ARI of the computed cluster assignments (see Appendix for details).

4.1.1 Comparison with state-of-the-art baselines

In our comparison, we considered some state-of-the-art methods that are developed for image clustering problems and are targeting end-to-end training scenarios from random initialization.

TABLE 3: Dataset Summary

Dataset	Classes	Split	Samples	Resolution
ImageNet-10	10	train	13000	160 × 160
ImageNet-Dogs	15	train	19500	160×160
STL-10	10	train+test	13000	96× 96
CIFAR-10	10	train	50000	32× 32
CIFAR100-20	20	train	50000	32× 32

We should note that we do not consider baselines that use prior information e.g.nearest neighbors derived by using pre-trained models. The implementation details of ConCURL are provided in Appendix and the results are presented in Table 4.

We observe that ConCURL outperforms the baseline algorithms considered on all the three metrics in all the data sets except STL-10 . ConCURL improves the state-of-the art clustering accuracy by app. 17.5% on ImageNet-Dogs , by 12.7% on CIFAR100-20 and by 3.8% on CIFAR-10 . Although ConCURL improves over ID [19], please note that ID is backbone used in this paper, and slightly worse than IDFD as shown in [19].

The proposed method achieves good clustering performance on popular computer vision datasets. Similar to all the algorithms considered, we assume that "K - the number of clusters" are known. However, this may not hold true in practice in real world applications. In such a case, we may assume an estimate of upper bound on the number of clusters to use as the number of prototypes. Additionally, we also assume that the dataset is equally distributed among the "K" clusters. If this assumption (also common in literature [16], [18]) does not hold, the fast Sinkhorn-Knopp algorithm used to solve Eq. 3 may not be optimal.

4.1.2 Class specific accuracy

We present class specific percentage accuracy and confusion matrix in figure 3. In each row i, j^{th} entry in the matrix represents a percentage of samples from category i belong to the cluster of category j. For better visualization we round the percentage to the nearest integer. For perfect clustering, all elements in the diagonal should be equal to 100. Here we note some interesting observations. In ImageNet-10, airliner is the worst performing category where 7% samples of airliner category are confused with airship category. Also, 4% of samples from orange category are categorized as soccer ball. In ImageNet-Dogs, there are three spaniel type of dogs - blenheim spaniel, brittany spaniel and welsh springer spaniel which look very similar to each other. 19% samples from blenheim spaniel category are categorized as brittany spaniel and 5% as welsh springer spaniel. Similarly, 16% samples from brittany spaniel category are categorized as blenheim spaniel and welsh springer spaniel each. 44% samples from welsh springer spaniel category are categorized as brittany spaniel and 15% as blenheim spaniel. Kelpie and doberman are also confused with each other where 39% samples from kelpie

TABLE 4: Clustering with max-performance

Method		STL-10)	Im	ageNet-	-10	Ima	geNet-I	Oogs	С	IFAR-1	0	CI	FAR100)-20
Wichiod	ACC	NMI	ARI	ACC	NMI	ARI	ACC	NMI	ARI	ACC	NMI	ARI	ACC	NMI	ARI
k-means [36]	0.192	0.125	0.061	0.241	0.119	0.057	0.105	0.055	0.020	0.229	0.087	0.049	0.130	0.084	0.028
SC [37]	0.159	0.098	0.048	0.274	0.151	0.076	0.111	0.038	0.013	0.247	0.103	0.085	0.136	0.090	0.022
AC [38]	0.332	0.239	0.140	0.242	0.138	0.067	0.139	0.037	0.021	0.228	0.105	0.065	0.138	0.098	0.034
NMF [39]	0.180	0.096	0.046	0.230	0.132	0.065	0.118	0.044	0.016	0.190	0.081	0.034	0.118	0.079	0.026
AE [40]	0.303	0.250	0.161	0.317	0.210	0.152	0.185	0.104	0.073	0.314	0.239	0.169	0.165	0.100	0.048
SDAE [41]	0.302	0.224	0.152	0.304		0.138	0.190	0.104	0.078	0.297	0.251	0.163	0.151	0.111	0.046
DeCNN [42]	0.299	0.227	0.162	0.313	0.186		0.175	0.098	0.073	0.282	0.240	0.174	0.133	0.092	0.038
JULE [43]	0.277	0.182	0.164	0.300		0.138	0.138	0.054	0.028	0.272	0.192	0.138		0.103	0.033
DEC [44]	0.359	0.276	0.186	0.381	0.282	0.203	0.195	0.122	0.079	0.301	0.257	0.161	0.185	0.136	0.050
DAC [45]	0.470	0.366	0.257	0.527	0.394	0.302	0.275	0.219	0.111	0.522	0.396	0.306	0.238	0.185	0.088
DeepCluster [46]	0.334	N/A	N/A	N/A	N/A	N/A	N/A	N/A	N/A	0.374	N/A	N/A	0.189	N/A	N/A
DDC [47]	0.489	0.371	0.267	0.577	0.433	0.345	N/A	N/A	N/A	0.524	0.424	0.329	N/A	N/A	N/A
IIC [48]	0.610	N/A	N/A	N/A	N/A	N/A	N/A	N/A	N/A	0.617	N/A	N/A	0.257	N/A	N/A
DCCM [49]	0.482	0.376	0.262	0.710	0.608	0.555	0.383	0.321	0.182	0.623	0.496	0.408	0.327	0.285	0.173
GATCluster [50]	0.583	0.446	0.363	0.762	0.609	0.572	0.333	0.322	0.200	0.610	0.475	0.402	0.281	0.215	0.116
PICA [33]	0.713	0.611	0.531	0.870	0.802	0.761	0.352	0.352	0.201	0.696	0.591	0.512	0.337	0.310	0.171
CC [21]	0.850	0.746	0.726	0.893	0.859	0.822	0.429	0.445	0.274	0.790	0.705	0.637	0.429	0.431	0.266
ADC [51]	0.530	N/A	N/A	N/A	N/A	N/A	N/A	N/A	N/A	0.325	N/A	N/A	0.160	N/A	N/A
ID [19]	0.726	0.64	0.526	0.937	0.867	0.865	0.476	0.47	0.335	0.776	0.682	0.616	0.409	0.392	0.243
IDFD [19]	0.756	0.643	0.575	0.954	0.898	0.901	0.591	0.546	0.413	0.815	0.711	0.663	0.425	0.426	0.264
ConCURL	0.749	0.636	0.566	0.958	0.907	0.909	0.695	0.63	0.531	0.846	0.762	0.715	0.479	0.468	0.3034

are categorized as doberman and 29% samples from doberman are categorized as kelpie. In CIFAR-10 , 33% of samples from dog category are categorized as cat and 16% of samples from cat category are categorized as dog.

In STL-10 , none of the samples from cat category are sampled correctly. Even though STL-10 and CIFAR-10 have same list of categories, STL-10 seems harder to cluster compared to CIFAR-10 . Note that STL-10 has only 13000 images to learn representations while in CIFAR-10 , 60000 images were used. In CIFAR100-20 , none of the samples from aquatic mammals were categorized correctly. 37% samples from aquatic mammals were categorized as fish and 19% as large omnivores and herbivores. In the case of reptiles, only 15% examples were categorized correctly but 23% were categorized as fish, 16% as large carnivores and 13% as insects. Surprisingly 28% of samples from trees are categorized as aquatic mammals.

4.2 Cluster Visualizations

In this section, we provide two visualization of ImageNet-10 dataset. In figure 4, each row represents a randomly drawn images from each cluster. Images which have red plus yellow border are categorized wrongly and should belong to different cluster. For example, first image in the fourth row should have been in the truck category but it was categorized as airliner. In soccer ball category there are two mistakes where first image should have been categorized as truck and fourth image should have been categorized as dog. In ninth row, last image should have been categorized as airship but it was categorized as truck.

To check if learned representations closer to each other belong to the same category we use retrieval task. In figure 5, we show the results. First image of each row is used as a query (randomly samples from the dataset) and nearest five images to the query image were retrieved using their representations. Ideally one would expect that all retrieved images belong the category of query image. In the soccer ball category, first image retrieved does not belong to it but both images have water as their main feature. In the last row, second image retrieved is a penguin, and ideally should not have been closer to the orange category.

4.3 Cross Model accuracy (out of distribution)

Here we calculate the clustering perfomance when the model is trained on one dataset but evaluated on a different dataset which may have different number clusters. For example, first row in table 5 gives performance of model trained on ImageNet-10 and evaluated on both ImageNet-10 and ImageNet-Dogs . Similarly second row gives performance of model trained on ImageNet-Dogs . We found that ImageNet-10 performance was decreased to 37% when model trained on ImageNet-Dogs was used instead of ImageNet-10 . Similarly ImageNet-Dogs performance was decreased to 25% when model trained on ImageNet-10 was used instead of ImageNet-Dogs . Table 6 gives the same perfomance metric for CIFAR-10 and CIFAR100-20. It is clear that these performance drops are significant and the generalization performance of learned embedding needs to be assessed by taking into account out of distribution data sets. However, since there are only 2 sets of different data sets it is hard to reach a definitive conclusion. Hence, in the following section we propose a new evaluation methodology which will shed light to out of distribution performance of learned embeddings.

TABLE 5: ImageNet-10 vs ImageNet-Dogs cross model performance

Model Trained on	ImageNet-10			ImageNet-Dogs		
Wiodel Trained on	ACC	NMI	ARI	ACC	NMI	ARI
ImageNet-10	0.958	0.908	0.910	0.177	0.127	0.068
ImageNet-Dogs	0.356	0.298	0.184	0.695	0.630	0.532

TABLE 6: CIFAR-10 vs CIFAR100-20 cross model performance

Model Trained on		IFAR-1		CIFAR100-20			
Woder Trained on	ACC	NMI	ARI	ACC	NMI	ARI	
CIFAR-10	0.846	0.762	0.715	0.178	0.158	0.061	
CIFAR100-20	0.464	0.359	0.250	0.480	0.468	0.304	

4.3.1 ImageNet-10-random and ImageNet-15-random accuracies

Here we compare the baseline model trained with ID [6] with our proposed method ConCURL. We randomly sample 10 and 15 classes from 1000 class ImageNet and evaluate the clustering

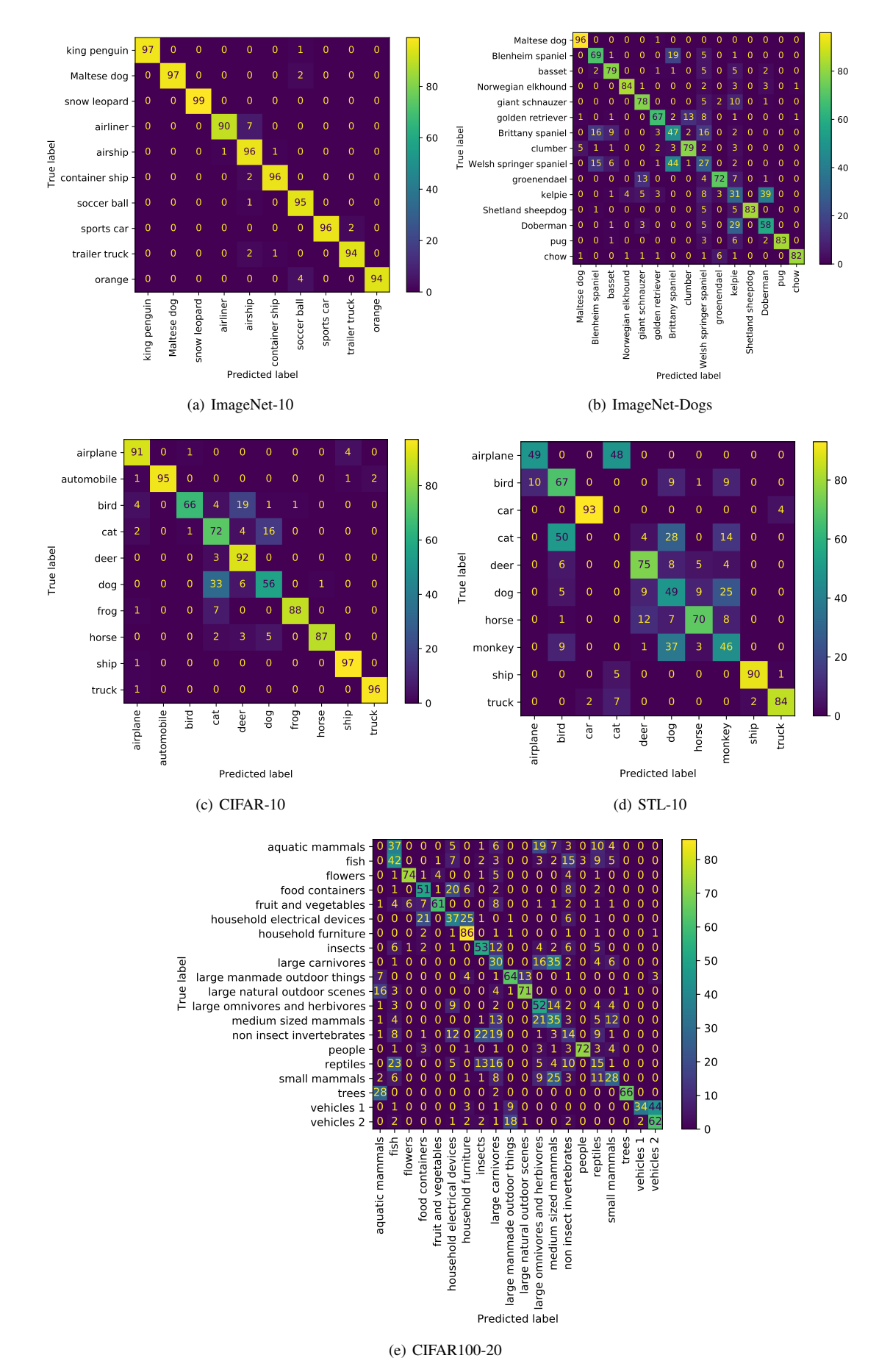


Fig. 3: Confusion Matrix

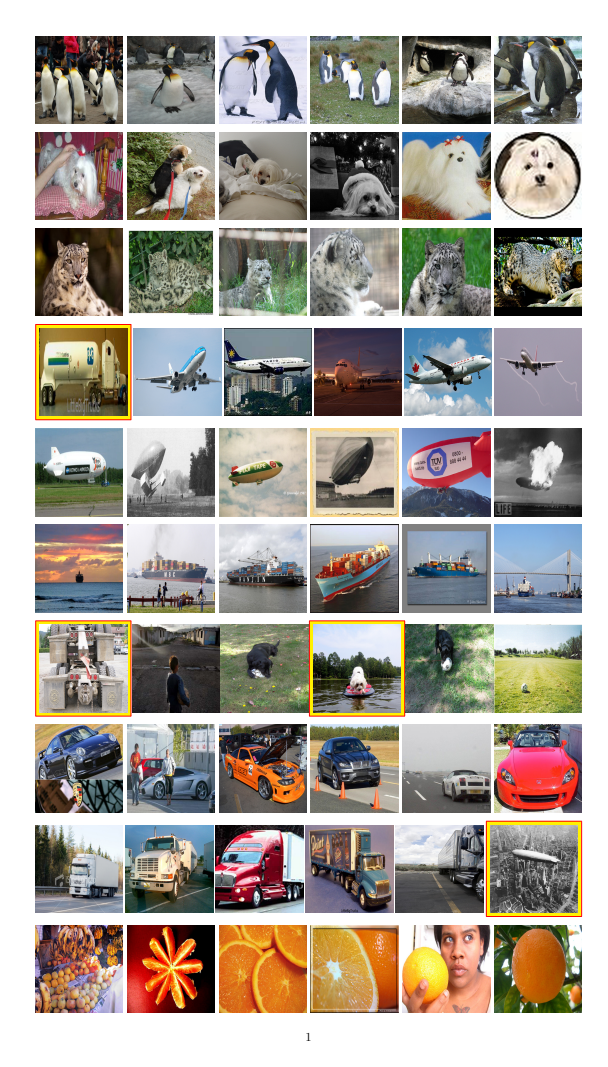


Fig. 4: Images from same cluster

accuracy on train split of the data using model trained from original ImageNet-10 and ImageNet-Dogs . We repeat the process 100 times for both 10 classes and 15 classes dataset and call it a random-10 and random-15 dataset respectively. Note that we don't retrain the model on the randomly sampled dataset but we only evaluate on it. We show the histogram of the accuracies we got in these 100 random datasets. In figure 6, we compare accuracy on both random-10 and random-15 for ConCURL model and baseline ID model trained on ImageNet-10. Along with histogram we show Gaussian distribution (in red dotted line) with first and second moment equal to average and standard deviation of of all accuracies respectively. Similarly in figure 7 we show accuracies based on models trained on ImageNet-Dogs . For models trained on ImageNet-10, baseline ID model performs slightly better compared to the proposed ConCURL model. The trend is reversed for the evaluation based on model trained on ImageNet-Dogs where ConCURL performs better compared to the baseline model. Even though proposed method performs best in max-performance it performs slightly worse on random-10. This result strengthens our argument of the need of going beyond traditional reporting of max-performance based on Acc, NMI and ARI.



Fig. 5: Retrieved images given a query image

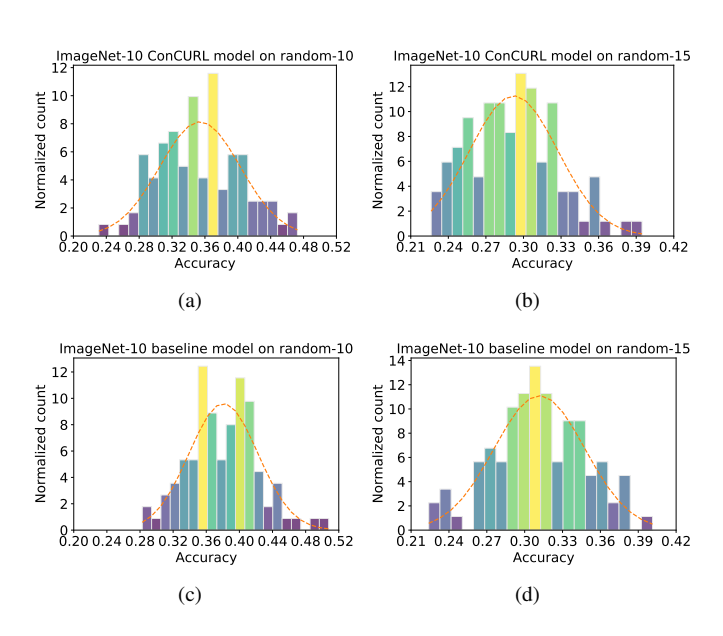


Fig. 6: Histogram of clustering accuracies for models trained on ImageNet-10 , (a) ConCURLmodel evaluated on random-10, (b) ConCURLmodel evaluated on random-15, (c) Baseline (ID) model evaluated on random-10, (d) Baseline (ID) model evaluated on random-15

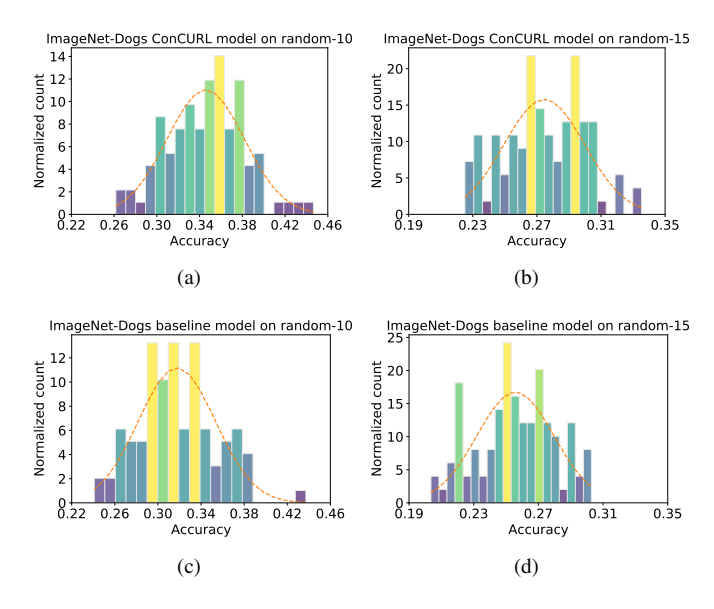


Fig. 7: Histogram of clustering accuracies for models trained on ImageNet-Dogs , (a) ConCURLmodel evaluated on random-10, (b) ConCURLmodel evaluated on random-15, (c) Baseline (ID) model evaluated on random-10, (d) Baseline (ID) model evaluated on random-15

5 ABLATION STUDIES

Although the proposed method is trained end-to-end, each different component of the method may have different impact. We have conducted five controlled experiments to quantify impact of used effect of data augmentations (Section 5.1), image resolution (Section 5.2), the number of transformations (Section 5.3), the dimension of transformation (Section 5.3) and architecture choice (Section 5.4).

5.1 Effect of Data Augmentations (DA)

TABLE 7: Data Augmentation Details

DA Type	Abbreviation	CIFAR-10	CIFAR100-20
All Data augmentations	All DA	0.8459	0.4798
No random horizontal flip	No RHF	0.7689	0.4551
No random gray scale	No RGS	0.7750	0.4357
No random apply blur	No RAB	0.7907	0.4295
No color jitter	No CJ	0.6463	0.2536
No random resized crop	No RRC	0.2988	0.1322

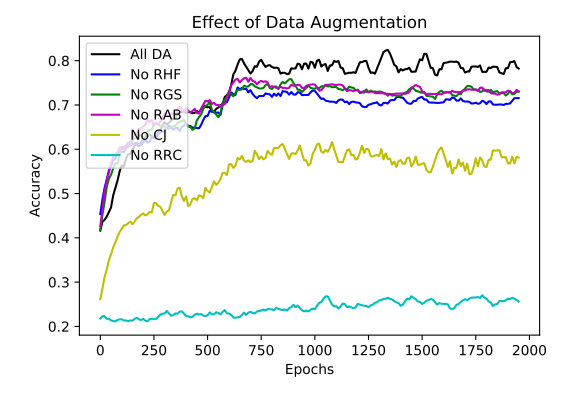


Fig. 8: Effect of data augmentation on CIFAR-10

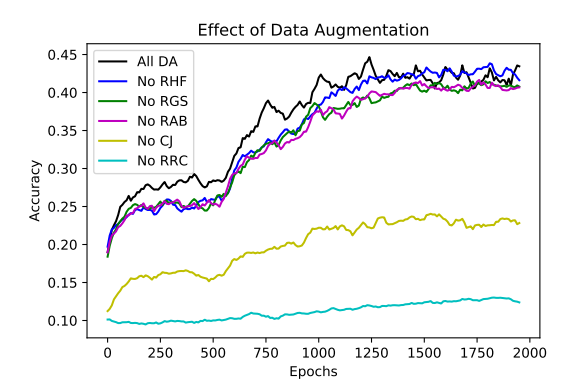


Fig. 9: Effect of data augmentation on CIFAR100-20

Augmenting the training data is a standard technique for training deep learning methods [52]. The backbones used in this study rely on the different views that are generated by applying different augmentations to the input image. Recently [53] has investigated the impact of data augmentation for contrastive learning methods and shed some light to the topic. In our setting, we would like to quantify the impact of data augmentations on Consensus loss. In the table 7, we show the maximum accuracy achieved when all data augmentations used and when we skip one data augmentation technique at a time. When all data augmentations are used maximum accuracy achieved is 0.8459 and 0.4798 on CIFAR-10 and CIFAR100-20 respectively. When random resized crop data augmentation is dropped, we have the maximum drop in the accuracy in both datasets followed by color jitter. Other data augmentation techniques are important to get the best possible accuracy but do not have as much effect as color jitter and random resized crop. In figures 8 and 9, we show how the running mean of accuracy progresses during training for each of the experiment in the table 7.

5.2 Effect of image resolution

TABLE 8: Effects of different resolutions for STL-10 , ImageNet-10 and ImageNet-Dogs .

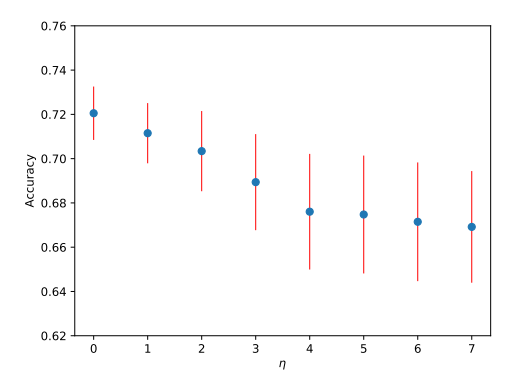
	32	64	96	160	224
STL-10	0.531	0.724	0.749	NA	NA
ImageNet-10	NA	NA	0.887	0.958	0.946
ImageNet-Dogs	NA	NA	0.629	0.695	0.679

Image resolution is often considered a free parameter and its effect on clustering performance not evaluated rigorously [19], [50]. We try to quantify the effect of different resolutions to the extent possible, given that some datasets are available only in specific resolutions. For STL-10 we have used 32×32 , 64×64 and 96×96 as resolutions. For ImageNet-10 and ImageNet-Dog-15 we have used 96×96 , 160×160 and 224×224 as resolutions. The results are given in Table 8.

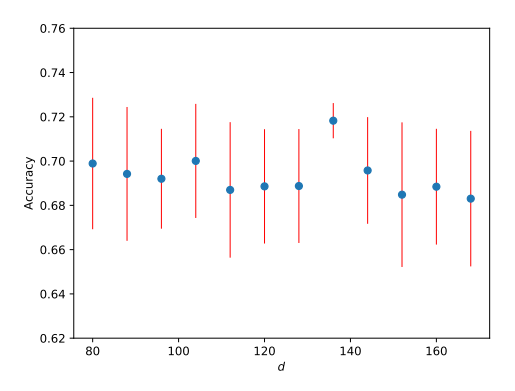
The best performance for ImageNet-10 and ImageNet-Dogs was at resolution 160 and for STL-10 it was at resolution 96. It is not clear why ImageNet-10 and ImageNet-Dogs did not perform the best at high resolution and further investigation is needed which we keep it as an open problem.

5.3 Components of Consensus Loss

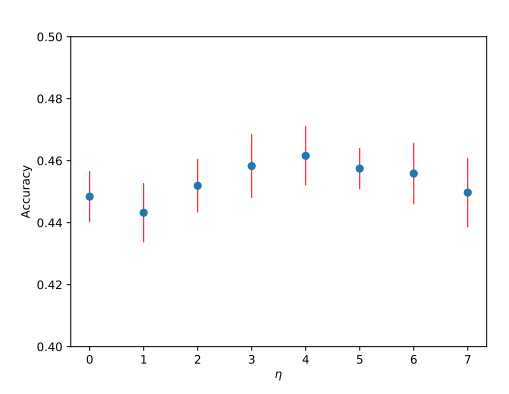
The proposed consensus loss has two parameters. First one is the number of transformations used and the second one is the



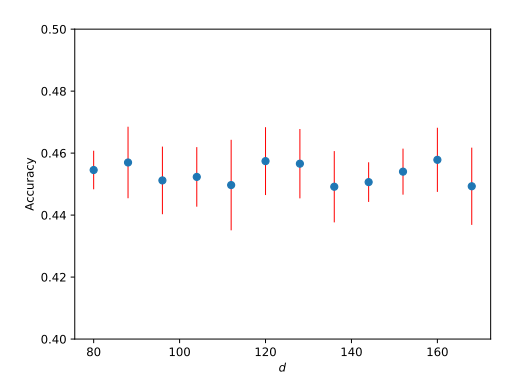
(a) STL-10: log of number of transformations



(b) STL-10 dimension of projection space



(c) CIFAR100-20 log of number of transformations



(d) CIFAR100-20 dimension of projection

Fig. 10: Components of consensus loss: ablation of STL-10 and CIFAR100-20

TABLE 9: Hyperparamers and the range values used for the experiments

	min	max	step size
τ = temperature parameter	0.3	1	0.1
l = learning rate	0.015	0.09	0.015
η = natural log of number of transformations	0	7	1
d = dimension of projection space	80	168	8

TABLE 10: Hyperparameters for max-performance

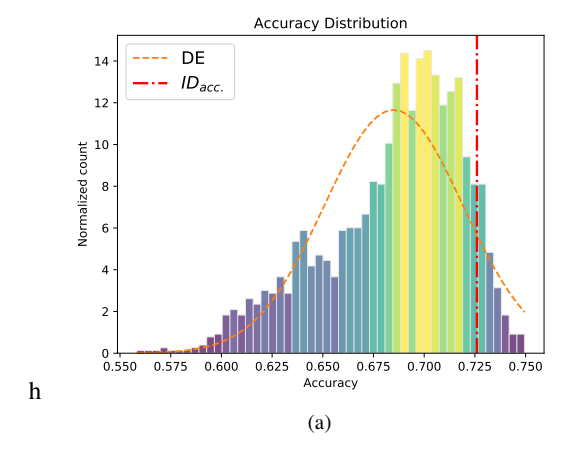
	STL-10	ImageNet-10	ImageNet-Dogs	CIFAR-10	CIFAR100-20
τ	0.8	1.0	0.5	0.85	0.35
l	0.03	0.03	0.06	0.015	0.06
$\exp(\eta)$	4	1	64	64	16
d	80	104	136	152	32

dimension of projection space. To understand the proposed loss, we have conducted a detailed experimental study on STL-10 and CIFAR100-20³. The used hyper-parameters are given in Table 9.

Due to the sheer number of conducted experiments, we will supply a summary statistics on a random set. We report empirical mean and standard deviation of marginal distribution of the quantity under investigation. Let $P_{\tau,\eta,d,l}$ be the joint distribution over hyperparameters τ (temperature parameter), l (learning rate), η (natural log of number of transformations) and d (dimension of projection space). We consider n_h as number of distinct values used in experiment for each hyperparameter $h \in \{\tau, \eta, d, l\}$ based on Table 9. We denote accuracy from each experiment based on the hyperparameters used as $a_{ au,\eta,d,l}$ Let $P_{h_i|h_j}$ be the conditional marginal distribution of hyperparameter h_i given h_j and conditional empirical mean of $P_{h_i|h_i}$ be $m(P_{h_i|h_i})$. In this case conditional empirical mean $m(P_{h_i|h_j})$ when $h_i=d$ and $h_j=\tau$ can be calculated using $m(P_{d|\tau})=\frac{1}{n_\eta\times n_l}\sum_{\eta}\sum_{l}a_{\tau,\eta,d,l}$. Consider the conditions of the calculated using $m(P_{d|\tau})=\frac{1}{n_\eta\times n_l}\sum_{l}a_{\tau,\eta,d,l}$. ditional empirical mean and standard deviation of other hyperparameters is calculated in the same way. In the figure 10, we show conditional empirical mean with blue dot and red line around the dot represents a standard deviation. For both, STL-10 and CIFAR100-20, we see the trend in number of projections. In STL-10, smaller the number of random projections, better it is and in CIFAR100-20 increasing random projections is helpful for the clustering accuracy upto some point. Note that when number of random projections is equal to zero, our setting is equivalent to baseline ID and we always perform better than ID. This means optimal number of random projections is greater or equal to one. There is no such a clear trend in number of dimensions of random projections.

Max-performance procedure is giving some insights to the performance of the algorithms at hand albeit it is not providing the whole picture because it is not considering the robustness of the performance differences. In Table 10, we give the hyperparameters that gave us the max-performance which does not give the complete picture of the robustness of the performance. In other words, just finding a hyper-parameter set which is giving better performance than the baseline is the core idea behind max-performance procedure. We ask the following question: given a hyper-parameter grid, how likely to get a better accuracy than the baseline? In Figure 11, we report the empirical accuracy distribution for STL-10 and CIFAR100-20 for all hyper-parameters given in Table 9. The red dotted lines show the corresponding baseline accuracy for each dataset. For STL-10 only app. 12.5% of the

^{3.} We have conducted similar but a smaller study on remaining data set and we have observed similar trends.



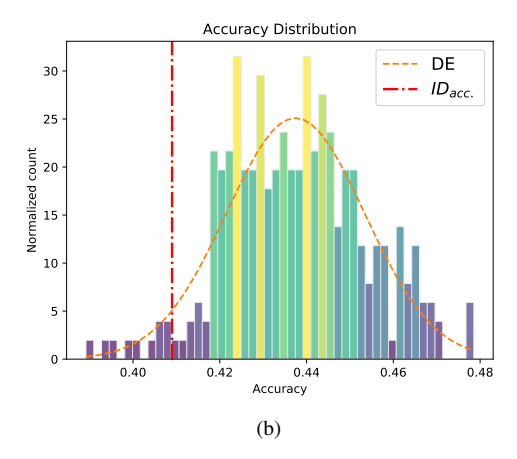


Fig. 11: The dotted red lines show the accuracy of baseline,i.e. ID [19], on the corresponding data set and DE is the density estimate of the empirical distribution. (a)Empirical accuracy distribution for STL-10 (b)Empirical accuracy distribution for CIFAR100-20 .

hyper-parameter sets gave better results than the baseline. On the other hand, for CIFAR100-20 , app. 90% of the hyper-parameter sets gave better results than the baseline. In other words, it doesn't require significant amount of computational power to find a better model than state-of-the art models for CIFAR100-20 however the situation is opposite for STL-10 . The results given in Figure 11 suggests that for comparing models multiple metrics need to be considered not only max-performance procedure.

5.4 Effect of architecture choice

In this work we have used ResNet-18 and ResNet-50 as network architectures. For both ResNet-18 and ResNet-50 we sweep over the same set of hyper parameter choices i.e., temperature, number of projections and projection dimension and report the results. Figure 12 shows the distribution of Δ_{acc} which is defined as accuracy difference between ResNet-50 and ResNet-18. Figure 12 indicates that ResNet-50 slightly outperforms ResNet-18, i.e. the mean difference is app. 0.5%.

6 CONCLUSION

In this work, we introduced different notions of consistency constraints that are enforced in different unsupervised/self-supervised learning algorithms. We propose a novel clustering algorithm

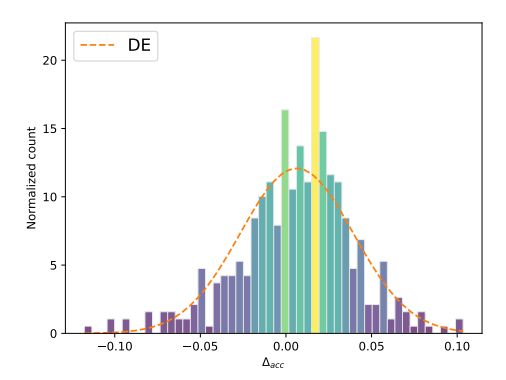


Fig. 12: Empirical distribution of performance difference between ResNet-50 and ResNet-18. DE is the density estimate of the empirical distribution.

that incorporates all three consistency constraints (exemplar, population and consensus) seamlessly and achieves state-of-the-art results in clustering for four out of five popular and challenging computer vision datasets. Our work on consensus clustering is significantly different from earlier consensus clustering works that do not learn representations. Moreover, we initiate a discussion on the adequacy of the currently used methods for evaluating clustering algorithms. We significantly extend the evaluation procedure of clustering algorithms that reflects the challenges of applying clustering to real world tasks.

APPENDIX A EVALUATION METRICS

We evaluate our algorithm by computing traditional clustering metrics (Cluster Accuracy, Normalized Mutual Information, and Adjusted Rand Index) which we discuss below in detail.

A.1 Cluster Accuracy

The clustering accuracy is computed by first computing a cluster partition of the input data. Once the partitions are computed and cluster indices assigned to each input data point, the linear assignment map is computed using Kuhn-Munkres (Hungarian) algorithm that reassigns the cluster indices to the true labels of the data. Clustering accuracy is then given by

$$ACC = \frac{\sum_{i=1}^{N} \mathbb{I}\{y_{true}(x_i) = c(x_i)\}}{N},$$

where $y_{true}(x_i)$ is a true label of x_i and $c(x_i)$ is the cluster assignment produced by an algorithm (after Hungarian mapping).

A.2 Normalized Mutual Information

For two clusterings U,V, with each containing |U|,|V| clusters respectively, and let $|U_i|$ be the number of samples in cluster U_i of clustering U (similarly for V), Mutual Information (MI) is given by

$$MI(U, V) = \sum_{i=1}^{|U|} \sum_{j=1}^{|V|} \frac{|U_i \cap V_i|}{N} \log \frac{N|U_i \cap V_j|}{|U_i||V_j|}$$

where N is the number of data points under consideration. Normalized Mutual Information is defined as

$$NMI(U,V) = \frac{MI(U,V)}{\sqrt{MI(U,U)MI(V,V)}}$$

A.3 Adjusted Rand Index

⁴ Suppose R is the groundtruth clustering and S is a partition, the RI of S is given as follows. Let a be the number of pairs of elements that are in the same set in R as well as in S; b be the number of pairs of elements that are in different sets in R, and different sets in S. Then

$$RI = \frac{a+b}{\binom{n}{2}}$$

$$ARI = \frac{RI - \mathbb{E}[RI]}{\max(RI) - \mathbb{E}[RI]}$$

APPENDIX B IMPLEMENTATION DETAILS

In this section, we discuss the implementation of the proposed algorithm. We use Pytorch version 1.7.1 for the implementation. The ID block of the algorithm uses the code from the implementation of ID [6] available at https://github.com/zhirongw/lemniscate.pytorch. The repository uses Pytorch version 0.3, and appropriate changes were made to use it with the latest version of Pytorch. We used ResNet-18 and ResNet-50 blocks during our experiments. In the ID block, the ResNet architecture is modified as follows. The final fully connected layer consists of 128 dimensions instead of the usual 1000 dimensions. The output of the final fully connected layer proceeds to compute the NCE loss, and the feature representations (layer before the fully connected layer) are fed to the clustering part.

For the clustering part, the MLP projection head g consists of a hidden layer of size 2048, followed by batch normalization and ReLU layers, and an output layer of size 256. The prototypes are thus chosen to be of dimension 256. Note that we fixed the number of prototypes to be equal to the number of ground truth classes of the dataset. It was shown however that over-clustering leads to better representations [11], [15], [26] and we can extend our model to include an over-clustering block with a larger set of prototypes [15] and alternate the training procedure between the blocks.

We train the algorithm for 2000 epochs for all datasets. We use SGD optimizer with a learning rate decay of 0.1 at pre-specified epochs (600, 950, 1300, 1650, 2000) to perform the updates for all datasets. We performed a coarse learning rate search and found 0.03 to be best performing. We used a batch size of 128 for all the datasets. To evaluate the cluster accuracy, we computed cluster assignments using MiniBatchKMeans⁵ with a batch size of 6000 and 20 random initializations.

B.0.1 Image Augmentations

The different views $\mathcal{X}_b^1, \mathcal{X}_b^2$ are not the same as views in multi-view datasets [54]. The views referred to in this paper correspond to different augmented views that are generated by image augmentation techniques, such as 'RandomHorizontalFlip', 'RandomCrop'. We explain the generation of multiple augmented views that are shown to be very effective in unsupervised learning [9]. Indeed it is possible to use more than two augmented views, but we limit to two for the sake of simplicity. [11] propose an

augmentation technique (Multi-Crop) to use more than two views. In this work, we use the augmentations used in [9], [10]. We first crop a random patch of the image with scale ranging from 0.08 to 1.0, and resize the cropped patch to 224×224 (96×96 in the case of smaller resolution datasets such as STL10). The resulting image was then flipped horizontally with a probability of 0.5. We then apply color transformations, starting by applying gray-scale with a probability of 0.2 followed by randomly changing the brightness, contrast, saturation and hue with a probability of 0.8. Then we applied a Gaussian Blur with kernel size (23×23) and a sigma chosen uniformly randomly between 0.1 and 2.0. The probability of applying the Gaussian Blur was 1.0 for view 1 and 0.5 for view 2. During evaluation, we resized the image such that the smaller edge of the image is of size 256 (not required for STL, CIFAR10, CIFAR100-20), and a center crop is performed with the resolution mentioned in the main paper. We finally normalize the image channels with the mean and standard deviation computed on ImageNet. Additionally, during training, we also experimented with applying a Sobel filter after all the image augmentations are performed before the forward pass. Applying a Sobel filter reduces the number of channels of the input images to 2. We also experimented with augmenting the RGB images with the output of the Sobel transform, resulting in 5 channel input images. In both these cases, the input channels in the first convolution layer were modified accordingly. All image augmentations were computed using Pytorch's torchvision module available in version 1.7.1.

B.0.2 Random Transformations

To compute the random transformations on the embeddings \mathbf{z} , we followed two techniques. We used Gaussian random projections with output dimension d, and transformed the embeddings \mathbf{z} to the new space with dimension d. In Gaussian random projections, the projection matrix is generated by picking rows from a Gaussian distribution such that they are orthogonal. We also used diagonal transformation [31] where we multiply \mathbf{z} with a randomly generated diagonal matrix of the same dimension as \mathbf{z} . We initialized M random transformations at the beginning and are kept fixed throughout the training.

APPENDIX C COMPARISON WITH LOCAL AGGREGATION

Local Aggregation (LA) [7] builds on Non-parametric Instance Discrimination [6] and uses a robust clustering objective (uses a closest neighbors set generated using multiple runs of k-means) similar to consensus clustering to move statistically similar points closer in the representation space and dissimilar points farther away. They demonstrate that the learnt representations are better by evaluating using the linear evaluation protocol on ImageNet.

However, the performance of these features for clustering was not discussed. Since LA is in spirit similar to our work, we perform a study on the clustering performance of features learnt using LA 6 on ImageNet-10, ImageNet-Dogs datasets. The results are presented in Tables 11.

6. using official Pytorch implementation available a https://github.com/neuroailab/LocalAggregation-Pytorch/tree/master/config

^{4.} https://scikit-learn.org/stable/modules/clustering.html#adjusted-rand-score

https://scikit-learn.org/stable/modules/clustering.html#mini-batchkmeans

TABLE 11: Comparison with LA on ImageNet-10

Datasets	ImageNet-10			ImageNet-Dogs		
Method\Metrics	Acc	NMI	ARI	Acc	NMI	ARI
LA	0.393	0.346	0.213	0.201	0.133	0.06
ConCURL	0.958	0.907	0.909	0.695	0.63	0.531

We observe that the clustering performance of our proposed algorithm ConCURL is much better than the clustering performance of LA method. Note that clustering performance of ID features is better than LA and our algorithm further improves on the clustering performance of ID. One major difference between our work and LA is the way in which we generate the ensemble. Our approach allows us to control and measure the diversity of the ensemble which can be useful in making algorithm design choices. Although LA controls the ensemble by varying (number of clusterings) and (number of clusters in each clustering) which aptly suits the objective they are solving, their ensembles are limited to use k-means clustering (the authors show that other clustering approaches are either not scalable, or are not optimal). In our case, by applying feature space transformations, we have much more freedom in generating the ensemble. We used random projections, diagonal transformations, but there could be other transformations on the feature space that we have not explored yet.

C.1 Implementation Details of LA

We trained the model for 500 epochs. Since the original implementation was for ImageNet, we performed a hyper-parameter search as follows. Using the config file from the official PyTorch implementation and we created 36 configuration files by varying learning rate and kmeans 'k'. In the original config file of authors, kmeans-k = 30000 (for 1.28 million images). We scale the kmeans-k for ImageNet-10 (13000 images) and ImageNet-Dogs (19500 images) accordingly and try six different values. In particular, we try learning-rates = [0.003, 0.005, 0.01, 0.03, 0.05, 0.1], and kmeans-k = [10, 15, 100, 310, 452, 500].

The background neighbors are 4096 as used in the paper. We ran ResNet18 experiments for the full hyperparameter search (36 experiments) and evaluated the cluster metrics. Additionally, we chose the top 5 choices of hyperparameters from above, and also ran ResNet34 experiments with those parameters, for both the datasets. In Table 11, we present the best results for each dataset.

The code repository uses a different version of ResNet (Pre-ActResNet). Therefore, for evaluation of cluster performance, we take the output of the layer before the final dense layer. For ResNet18, the output dimensions of this layer is (512,7,7) and we take the mean along (1,2) dimensions and use the resulting 512 dimension vector. We compute k-means clustering on these embeddings using faiss (https://github.com/facebookresearch/faiss) for the train split of the data, and compute the cluster metrics as mentioned in our paper.

REFERENCES

- Y. LeCun, Y. Bengio, and G. Hinton, "Deep learning," *nature*, vol. 521, no. 7553, pp. 436–444, 2015.
- [2] B. J. Frey and D. Dueck, "Clustering by passing messages between data points," *science*, vol. 315, no. 5814, pp. 972–976, 2007.
- [3] F. Masulli and A. Schenone, "A fuzzy clustering based segmentation system as support to diagnosis in medical imaging," *Artificial intelligence* in medicine, vol. 16, no. 2, pp. 129–147, 1999.

- [4] A. K. Jain, M. N. Murty, and P. J. Flynn, "Data clustering: a review," ACM computing surveys (CSUR), vol. 31, no. 3, pp. 264–323, 1999.
- [5] R. Xu and D. Wunsch, "Survey of clustering algorithms," *IEEE Transactions on neural networks*, vol. 16, no. 3, pp. 645–678, 2005.
- [6] Z. Wu, Y. Xiong, S. X. Yu, and D. Lin, "Unsupervised feature learning via non-parametric instance discrimination," in *Proceedings of the IEEE Conference on Computer Vision and Pattern Recognition*, 2018, pp. 3733–3742.
- [7] C. Zhuang, A. L. Zhai, and D. Yamins, "Local aggregation for unsupervised learning of visual embeddings," in *Proceedings of the IEEE International Conference on Computer Vision*, 2019, pp. 6002–6012.
- [8] K. He, H. Fan, Y. Wu, S. Xie, and R. Girshick, "Momentum contrast for unsupervised visual representation learning," in *Proceedings of the IEEE/CVF Conference on Computer Vision and Pattern Recognition*, 2020, pp. 9729–9738.
- [9] T. Chen, S. Kornblith, M. Norouzi, and G. Hinton, "A simple framework for contrastive learning of visual representations," arXiv preprint arXiv:2002.05709, 2020.
- [10] J.-B. Grill, F. Strub, F. Altché, C. Tallec, P. H. Richemond, E. Buchatskaya, C. Doersch, B. A. Pires, Z. D. Guo, M. G. Azar et al., "Bootstrap your own latent: A new approach to self-supervised learning," arXiv preprint arXiv:2006.07733, 2020.
- [11] M. Caron, I. Misra, J. Mairal, P. Goyal, P. Bojanowski, and A. Joulin, "Unsupervised learning of visual features by contrasting cluster assignments," arXiv preprint arXiv:2006.09882, 2020.
- [12] M. Caron, P. Bojanowski, A. Joulin, and M. Douze, "Deep clustering for unsupervised learning of visual features," in *Proceedings of the European Conference on Computer Vision (ECCV)*, 2018, pp. 132–149.
- [13] J. Xie, R. Girshick, and A. Farhadi, "Unsupervised deep embedding for clustering analysis," in *International conference on machine learning*, 2016, pp. 478–487.
- [14] S. A. Shah and V. Koltun, "Deep continuous clustering," arXiv preprint arXiv:1803.01449, 2018.
- [15] X. Ji, J. F. Henriques, and A. Vedaldi, "Invariant information clustering for unsupervised image classification and segmentation," in *Proceedings* of the IEEE International Conference on Computer Vision, 2019, pp. 9865–9874.
- [16] C. Niu, J. Zhang, G. Wang, and J. Liang, "Gatcluster: Self-supervised gaussian-attention network for image clustering," arXiv preprint arXiv:2002.11863, 2020.
- [17] J. Wu, K. Long, F. Wang, C. Qian, C. Li, Z. Lin, and H. Zha, "Deep comprehensive correlation mining for image clustering," in *Proceedings* of the IEEE International Conference on Computer Vision, 2019, pp. 8150–8159.
- [18] J. Huang, S. Gong, and X. Zhu, "Deep semantic clustering by partition confidence maximisation," in *Proceedings of the IEEE/CVF Conference* on Computer Vision and Pattern Recognition, 2020, pp. 8849–8858.
- [19] Y. Tao, K. Takagi, K. Nakata, and C. R. Center, "Clustering-friendly representation learn-ing via instance discrimination and feature decorrelation."
- [20] K. He, H. Fan, Y. Wu, S. Xie, and R. Girshick, "Momentum contrast for unsupervised visual representation learning," arXiv preprint arXiv:1911.05722, 2019.
- [21] Y. Li, P. Hu, Z. Liu, D. Peng, J. T. Zhou, and X. Peng, "Contrastive clustering," in AAAI, 2021.
- [22] W. Van Gansbeke, S. Vandenhende, S. Georgoulis, M. Proesmans, and L. Van Gool, "Scan: Learning to classify images without labels," 2020.
- [23] A. Strehl and J. Ghosh, "Cluster ensembles—a knowledge reuse framework for combining multiple partitions," *Journal of machine learning research*, vol. 3, no. Dec, pp. 583–617, 2002.
- [24] J. Ghosh and A. Acharya, "Cluster ensembles," Wiley Interdisciplinary Reviews: Data Mining and Knowledge Discovery, vol. 1, no. 4, pp. 305– 315, 2011.
- [25] X. Z. Fern and C. E. Brodley, "Random projection for high dimensional data clustering: A cluster ensemble approach," in *Proceedings of the* 20th international conference on machine learning (ICML-03), 2003, pp. 186–193.
- [26] Y. M. Asano, C. Rupprecht, and A. Vedaldi, "Self-labelling via simultaneous clustering and representation learning," arXiv preprint arXiv:1911.05371, 2019.
- [27] M. Cuturi, "Sinkhorn distances: Lightspeed computation of optimal transport," in Advances in neural information processing systems, 2013, pp. 2292–2300.
- [28] H. W. Kuhn, "The hungarian method for the assignment problem," Naval research logistics quarterly, vol. 2, no. 1-2, pp. 83–97, 1955.
- [29] ——, "Variants of the hungarian method for assignment problems," Naval Research Logistics Quarterly, vol. 3, no. 4, pp. 253–258, 1956.

- [30] A. L. Fred and A. K. Jain, "Combining multiple clusterings using evidence accumulation," *IEEE transactions on pattern analysis and machine intelligence*, vol. 27, no. 6, pp. 835–850, 2005.
- [31] K. Hsu, S. Levine, and C. Finn, "Unsupervised learning via metalearning," arXiv preprint arXiv:1810.02334, 2018.
- [32] A. K. Jain and R. C. Dubes, Algorithms for clustering data. Prentice-Hall, Inc., 1988.
- [33] J. Huang, S. Gong, and X. Zhu, "Deep semantic clustering by partition confidence maximisation," in CVPR, June 2020.
- [34] J. Deng, W. Dong, R. Socher, L.-J. Li, K. Li, and L. Fei-Fei, "Imagenet: A large-scale hierarchical image database," in 2009 IEEE conference on computer vision and pattern recognition. Ieee, 2009, pp. 248–255.
- [35] J. Chang, L. Wang, G. Meng, S. Xiang, and C. Pan, "Deep adaptive image clustering," in *The IEEE International Conference on Computer* Vision (ICCV), Oct 2017.
- [36] J. Macqueen, "Some methods for classification and analysis of multivariate observations," in In 5-th Berkeley Symposium on Mathematical Statistics and Probability, 1967, pp. 281–297.
- [37] A. Y. Ng, M. I. Jordan, and Y. Weiss, "On spectral clustering: Analysis and an algorithm," in *NeurIPS*, T. G. Dietterich, S. Becker, and Z. Ghahramani, Eds. MIT Press, 2002, pp. 849–856. [Online]. Available: http://papers.nips.cc/paper/2092-on-spectral-clustering-analysis-and-an-algorithm.pdf
- [38] P. Franti, O. Virmajoki, and V. Hautamaki, "Fast agglomerative clustering using a k-nearest neighbor graph," *IEEE Transactions on Pattern Analysis and Machine Intelligence*, vol. 28, no. 11, pp. 1875–1881, Nov 2006.
- [39] D. Cai, X. He, X. Wang, H. Bao, and J. Han, "Locality preserving nonnegative matrix factorization," in *IJCAI*, 2009, pp. 1010–1015. [Online]. Available: http://ijcai.org/Proceedings/09/Papers/171.pdf
- [40] Y. Bengio, P. Lamblin, D. Popovici, H. Larochelle, and U. Montreal, "Greedy layer-wise training of deep networks," *NeurIPS*, vol. 19, pp. 153–160, 2007.
- [41] P. Vincent, H. Larochelle, I. Lajoie, Y. Bengio, and P. A. Manzagol, "Stacked denoising autoencoders: Learning useful representations in a deep network with a local denoising criterion." *Journal of Machine Learning Research*, vol. 11, no. 12, pp. 3371–3408, 2010.
- [42] M. D. Zeiler, D. Krishnan, G. W. Taylor, and R. Fergus, "Deconvolutional networks," in *Computer Vision and Pattern Recognition*, 2010.
- [43] J. Yang, D. Parikh, and D. Batra, "Joint unsupervised learning of deep representations and image clusters," in CVPR, 2016.
- [44] J. Xie, R. Girshick, and A. Farhadi, "Unsupervised deep embedding for clustering analysis," in *ICML*, ser. ICML'16. JMLR.org, 2016, pp. 478–487. [Online]. Available: http://dl.acm.org/citation.cfm?id= 3045390.3045442
- [45] J. Chang, L. Wang, G. Meng, S. Xiang, and C. Pan, "Deep adaptive image clustering," in *ICCV*, Oct 2017, pp. 5880–5888.
- [46] M. Caron, P. Bojanowski, A. Joulin, and M. Douze, "Deep clustering for unsupervised learning of visual features." in ECCV, vol. 11218, 2018, pp. 139–156.
- [47] J. Chang, Y. Guo, L. Wang, G. Meng, S. Xiang, and C. Pan, "Deep discriminative clustering analysis," 2019.
- [48] X. Ji, J. F. Henriques, and A. Vedaldi, "Invariant information clustering for unsupervised image classification and segmentation," in *ICCV*, October 2019.
- [49] J. Wu, K. Long, F. Wang, C. Qian, C. Li, Z. Lin, and H. Zha, "Deep comprehensive correlation mining for image clustering," in *ICCV*, October 2019.
- [50] C. Niu, J. Zhang, G. Wang, and J. Liang, "Gatcluster: Self-supervised gaussian-attention network for image clustering," in ECCV, 2020, pp. 735–751.
- [51] P. Haeusser, J. Plapp, V. Golkov, E. Aljalbout, and D. Cremers, "Associative deep clustering: Training a classification network with no labels," in *Pattern Recognition*, T. Brox, A. Bruhn, and M. Fritz, Eds. Cham: Springer International Publishing, 2019, pp. 18–32.
- [52] C. Shorten and T. M. Khoshgoftaar, "A survey on image data augmentation for deep learning," *Journal of Big Data*, vol. 6, no. 1, pp. 1–48, 2010
- [53] Y. Tian, C. Sun, B. Poole, D. Krishnan, C. Schmid, and P. Isola, "What makes for good views for contrastive learning," arXiv preprint arXiv:2005.10243, 2020.
- [54] T. Schops, J. L. Schonberger, S. Galliani, T. Sattler, K. Schindler, M. Pollefeys, and A. Geiger, "A multi-view stereo benchmark with high-resolution images and multi-camera videos," in *Proceedings of the IEEE Conference on Computer Vision and Pattern Recognition*, 2017, pp. 3260–3269.